Chapter 15

Organic Solar Cells

Maria Isabel Alonso and Mariano Campoy-Quiles

Abstract

Organic solar cells attract both scientific and economic interest due to their potential for clean and cost-effective photovoltaic energy conversion. Continuous evolution of this field relies on materials research, including synthesis of new compounds and fine control over film microstructure, as well as improved device architectures. In this context, spectroscopic ellipsometry is a helpful characterization tool, stretching over material preparation, device structure, and device modelling. This chapter will provide a general perspective of aspects that can be investigated by ellipsometry in these systems. The acquired insights enhance our capability to understand and model the optoelectronic properties of photovoltaic devices.

M. I. Alonso, M. Campoy-Quiles
Institut de Ciència de Materials de Barcelona (ICMAB-CSIC), Campus UAB, 08193 Bellaterra, Spain.

15.1 Introduction

The field of organic solar cells or photovoltaics (OPV) is in continuous development mainly driven by its advantageous traits: environment-friendly low-cost generation of energy owing to the possibility of large area manufacturing of flexible, light-weight, semi-transparent devices with low energy payback times. Progress in this field is largely based on the design of new materials, control of microstructure and the improvement of device geometries. In this context, spectroscopic ellipsometry is gaining attention for the characterization and optimization of layered devices. The technique can be helpful to evaluate new active materials, obtain detailed depth profiles of material composition, and study solid-state microstructure of organic semiconductors, which can be very varied depending on the physical phase and molecular orientation, so that the device optical properties emerge as a combination of both chemical nature and solid state packing.

The device architectures developed for OPVs take into account the particular properties of organic semiconductors. Active layers must be thin to optimize the efficiency of charge extraction. This is partly due to the large binding energies of photoexcited electron-hole pairs (called excitons) and their short diffusion length, L_D ~20 nm, before recombination. Such excitons need to reach the p-n (or donor-acceptor, D-A) junction to dissociate into free charges. Once this charge transfer process happens, the charge extraction is also hindered by a very low charge-carrier mobility that limits the effective charge separation and collection. Since sufficient layer thickness is needed to absorb a reasonable amount of photons, in planar junctions a thickness compromise must be met. Fortunately, organic semiconductors have relatively strong absorption coefficients and operational thicknesses are not too large. It is also possible to tailor the active compounds via chemical synthesis to reach improved matching with the solar spectrum. The device architecture that addresses the mentioned drawbacks is the bulk heterojunction concept shown in Fig. 15.1, in which D and A compounds are blended to increase the available interface and to shorten the distance from any point to an interface. The morphology and phase separation in the blend are critical to OPV performance and in favorable cases can be evaluated by SE. As a non-invasive tool, SE can also be applied *in-situ* and in real-time to evaluate film deposition kinetics, to monitor temporal changes in morphology such as those occurring during post-deposition treatments, and even be an in-line monitoring tool to assess organic photovoltaic thin film microstructure during roll-to-roll processing. [1,2]

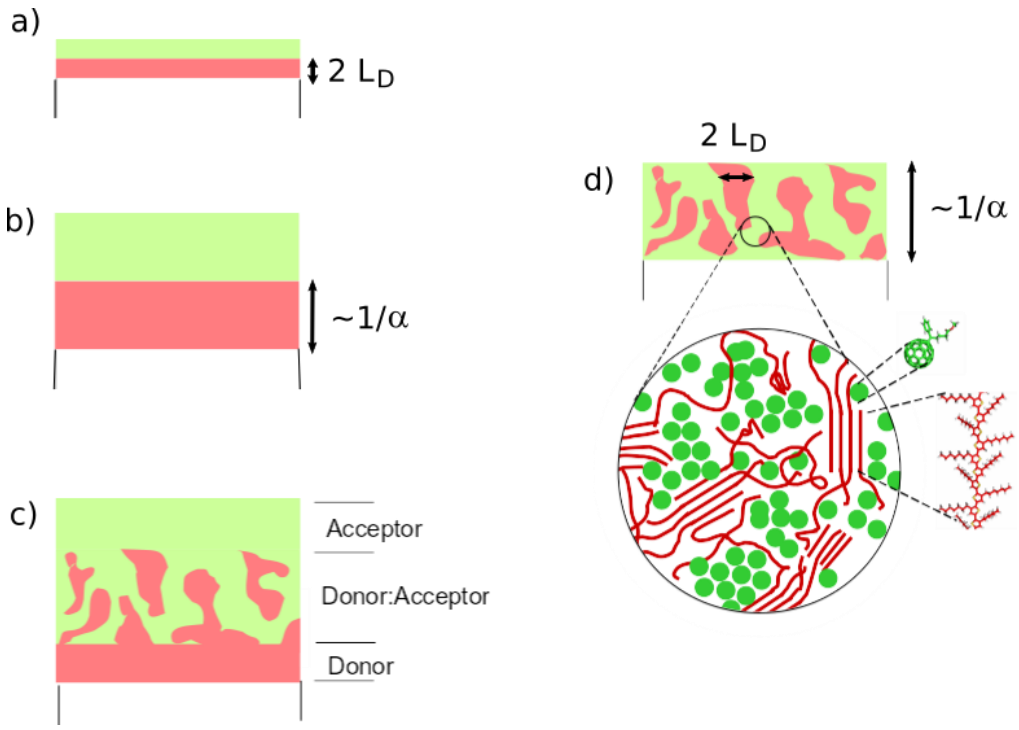

Fig. 15.1 Schematics of the active layer for several device configurations based on donor-acceptor (D-A) junctions. The main absorber is assumed to be the donor (red region). The two relevant lengths for planar junctions are given in a) and b), where L_D represents the exciton diffusion length and α the maximum value of absorption coefficient of the donor. c) Bulk heterojunction with vertical phase separation region which is detailed in d) assuming a P3HT:PCBM blend.

15.2 Ellipsometric Characterization of Organic Semiconductors

In this section, we focus on the optical properties of single-phase materials that form the active layers of OPVs. The visible range spectra of organic semiconductors generally exhibit several bands that predominantly comprise electronic transitions between π-electron levels and their vibronic sidebands. Measured transitions display lineshapes resulting from a Poisson distribution of the oscillator strength over the series of vibronic replicas, described by a Huang-Rhys parameter. The frequencies of vibrations that couple to electronic states are usually high, giving rise to large total bandwidths. The intermolecular interactions, different conformations or states of order further broaden the spectral features resulting in asymmetric absorption bands and shoulders. Commonly, the analysis of these vibronically structured peaks is kept simple and they are modelled as asymmetrically broadened electronic transitions.[3] Fitting of ellipsometric spectra of films has been already described in Chapter 3 and common strategies for the particular case of polymer semiconductors have been recently reviewed.[4] Here, we describe results obtained in different organic semiconductor materials. We consider first single crystal molecular semiconductors, as useful model substances. Then, we turn to thin films which are obtained using two main methodologies: thermal evaporation and solution processing. In all two cases the processing conditions or choice of the substrates have a large influence on the resulting microstructure, impacting the corresponding optical properties. Typically, molecules with low molecular weight are insoluble but relatively ordered films can be obtained by vacuum evaporation in favorable conditions. Crystal polymorphism is, however, an issue to be dealt with. For high molecular weights, typically polymeric chains, solution processing methods are employed and the resulting films are as a rule of thumb more disordered. Therefore, structural aspects acquire high importance when characterizing organic films for OPVs.

15.2.1 Single Crystals

The study of single crystal molecular materials is interesting from two perspectives. Firstly, it offers access to unique fundamental phenomena in solid state optical properties. Secondly, it provides helpful references to understand the optical properties of other organic semiconductors more common to OPV application. The main objective in single crystal ellipsometry is to determine the dielectric tensor. In the case of molecular single crystals this objective has been hampered by the lack of appropriate single crystals as well as by the difficulty of reliably determining the dielectric tensor of low symmetry crystals. Some OPV relevant single crystalline materials have been investigated using ellipsometry including for instance tetracene,[5] pentacene,[6] and fullerite (C_{60}).[7] The C_{60} crystal is cubic at room temperature and therefore optically isotropic. The rest of crystals are anisotropic, crystallize usually in monoclinic or triclinic systems and the dielectric tensor cannot be diagonalized in a fixed coordinate axes set.[8] Exact treatments taking into

account all degrees of freedom of the dielectric tensor allowed by symmetry have been applied in part of the spectrum to two prototypical organic semiconductors which are model compounds for organic optoelectronics: Anthracene and the perylene derivative PTCDA (perylene tetracarboxylic dianhydride). Both crystallize in monoclinic systems. Historically, the photovoltaic effect in organic semiconductors was first measured in anthracene. However, it is not currently used for OPV because of its high band gap, which is partly due to rather weak intermolecular interactions in the crystal leading to optical spectra of strong molecular character, as shown in Fig. 15.2. In spite of this, the crystalline molecular arrangement in anthracene, with a monoclinic angle of 124.7º, has a large impact into its dielectric tensor components. In particular, the phenomena of dispersion of principal axes of the dielectric tensor and non-coincidence for axes of the real and imaginary part of the tensor are well marked in anthracene.[9] The intermolecular interactions are stronger in PTCDA, for which the band character of the electronic structure is rather extended. The availability of detailed ellipsometric studies of single crystal PTCDA allowed testing refined theories of electronic structure of this class of semiconductors.[10] The monoclinic angle in PTCDA is 98.8º, close to orthogonal, but nevertheless the low symmetry manifests in the dielectric tensor.[11] In both mentioned examples the unit cells contain two molecules and the lowest singlet excitons display similar Davydov splittings (cf. Sect. 4.5.2) of the order of 40 meV. The observation of these fine splittings is considered a signature of crystalline perfection.

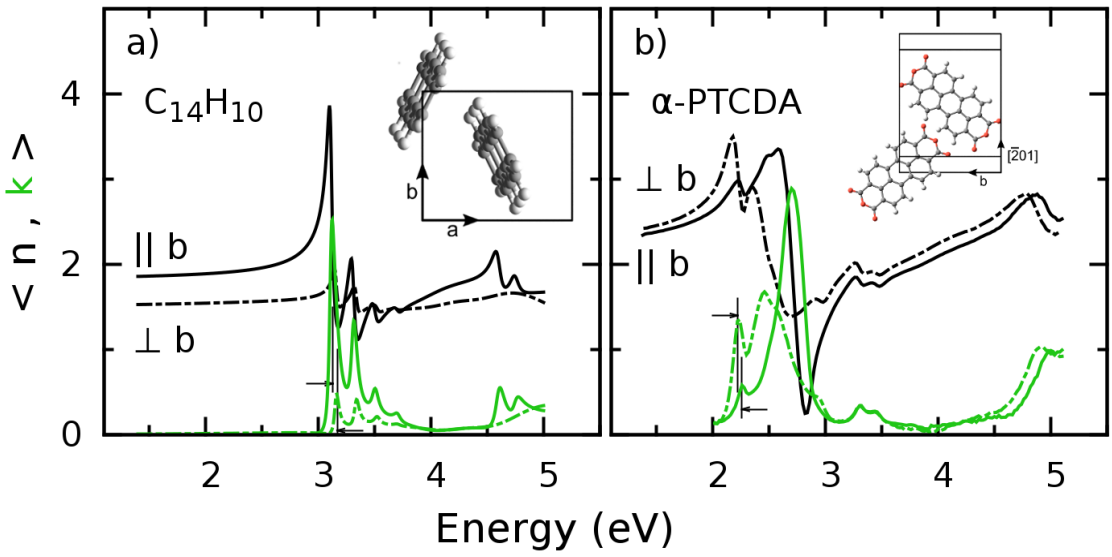

Fig. 15.2 Ellipsometric spectra of a) Anthracene (001) and b) α-PTCDA (102) single crystal cleaved surfaces given as pseudo-values < n > and < k >. The unit cells projected on the measured planes are given as insets. In both cases, the monoclinic b axis is on the plane and the unit cells contain two inequivalent molecules, giving rise to Davydov splittings. The latter are indicated on the lower excitonic peaks by vertical lines and arrows.

15.2.2 Vacuum Evaporated Films

The active layers in early OPV designs were composed by low molecular weight organic materials, i.e., small molecules or pigments. The initially studied structures were similar to inorganic devices, with planar heterojunctions deposited by thermal evaporation. The active films of these OPVs were usually combinations of metallo-phthalocyanines (MPc) with M = Cu, Zn acting as donor materials and perylene derivatives such as PTCBI (perylene tetracarboxylic bisbenzimidazole) and PTCDA acting as acceptors. An immediate evolution was to implement fullerenes C_{60} and later on C_{70} as acceptors since their spherical shape is advantageous to produce suitable blends with the mostly planar MPc molecules.[12] Hence, fullerenes remain the most chosen acceptors for bulk heterojunction (BHJ) devices despite their relatively limited spectral overlap with the solar spectrum. In the context of BHJs, the field of OPV is dominated by solution processed polymeric films (see Sect.15.2.3.). However, the more precise control both in molecule synthesis and purification, film morphology, and reproducibility in device fabrication offered by vacuum deposited small molecules maintains a sustained research activity in the field. Improvements in performance are seeked in multilayer architectures with multiple heterojunctions and tandem configurations. The increased complexity and cost of the multilayers should be balanced by a higher achievable efficiency. These systems are also regarded as models to obtain a fundamental understanding of the efficiency limiting mechanisms in OPVs. Compared to solution processing, upscaling can be more difficult for thermally evaporated systems needing vacuum. Roll-to-roll compatible vacuum technologies do, however, exist.

Ellipsometric characterization plays a central role in the development of new materials and improved structures, helping to evaluate both the spectral match and the film morphology, i.e., molecular orientation in films, polymorphism and interdiffusion between layers. The reference systems are MPc/fullerene combinations. Thus, research efforts to improve the overall spectral overlap with the solar spectrum are aimed to examine new donors as well as new acceptors to combine with fullerenes or to substitute them. In addition, optical anisotropy must be evaluated [13] to optimize in-plane absorption.[14] Even if the symmetry of single crystals is monoclinic or triclinic, films always display some disorder and the effective symmetry is at most orthorhombic [4] but normally is tetragonal. Hence, in most cases, only two components fully describe the uniaxial optical response of films with the most usual situation of the optic axis perpendicular to the film surface. Many donors other than MPcs have been considered including diindenoperylene (DIP),[13] squaraines,[15] as well as more complicated molecules designed with different moieties to tailor an improved performance.[16] Comparatively, less non-fullerene small molecule acceptors are capable of providing improved efficiencies. Among others, perfluorinated analogs of phthalocyanines [17] and subPcs [18] have been considered because fluorine acts as electron-withdrawing group and reduces the HOMO level of the molecules which become effective acceptors whereas the spectral match remains quite suitable. Figure 15.3 shows the anisotropic optical

functions of perfluorinated CuPc films. Different polymorphs result from deposition at different substrate temperatures: films deposited on unheated substrates display a spectrum similar to that of CuPc whereas films deposited on heated substrates show a strong redshifted exciton. Spectroscopic details can be related to the local arrangements of neighboring molecules. In all known CuPc polymorphs the molecular stacks are rather eclipsed forming H-aggregates. Such a redshifted exciton is the signature of staggered molecular stacks or J-aggregates, as observed in bulk F_{16}CuPc. Interestingly, the concepts of H- and J- aggregation have been extended to respectively describe interchain and intrachain coupling in conjugated polymers.[19]

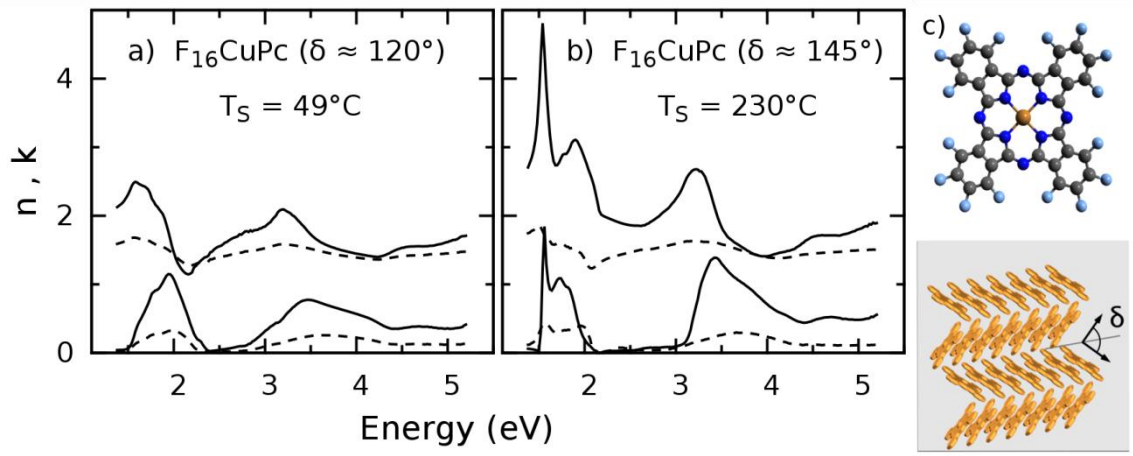

Fig. 15.3 Optical functions of two films of F_{16}CuPc deposited at different substrate temperatures. The observed effective optical anisotropy was uniaxial. Solid (dashed) lines give the ordinary (extraordinary) optical component obtained by point-by-point fitting. In a) the substrate was not directly heated, in b) it was kept at 230ºC. c) Schemes of the molecular structure and of the film arrangement, where different crystal polymorphs are given by the herringbone angle δ.

15.2.3 Solution Processed Films

As mentioned above, most organic films for OPVs are deposited from solution because this alternative offers many advantages, including low cost, high flexibility, low thermal budget and up-scalability. Different techniques such as spin coating, blade coating, inkjet printing and screen printing are often used to deposit conjugated polymers and soluble versions of small molecules. In particular the fullerene derivatives PCBM (Phenyl-C(60,70)-butyric acid methyl ester) depicted in Fig. 15.4 along with some usual donor polymers.

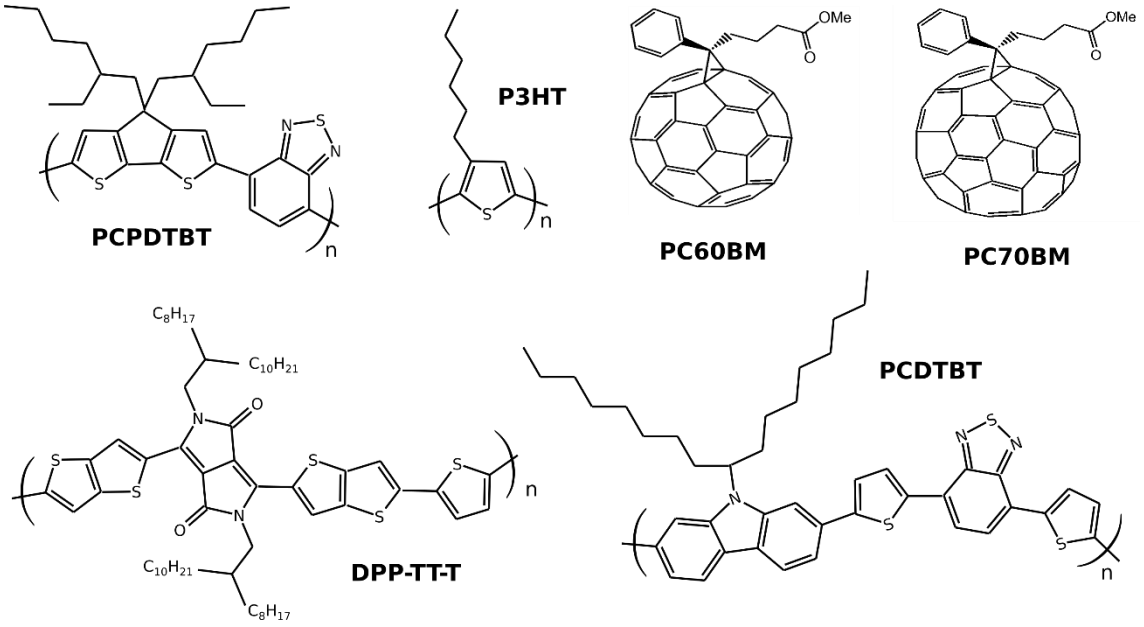

Fig. 15.4 Molecular structures of typical solution-processed OPV materials.

The optical properties of polymer films can be quite complex. In addition to the basic molecular nature of the polymer, the particular conformation is decisive to determine the effective optical properties of the film, given by both the spectral features (resulting from the electronic density of states) and the anisotropy (resulting from orientation). Even in a single-component film, a multi-phase morphology can occur. Because of the abundant morphological variations in polymers, it is pertinent to apply a physical parameterization of the dielectric function that allows describing structural variations and transformations by varying the model parameters. Systematic comparisons of the fitting quality of different dispersion models to the ellipsometry data for films of conjugated polymers coincide in concluding that asymmetric lineshapes are the most suited. The case of P3HT as the most important polymer in the context of OPV is illustrative. Arwin and Jansson [20] found that the best description of its optical properties was given by modified Lorentzian resonances which consist in adding a phase to a Lorentzian oscillator. This is a phenomenological approximation to account for asymmetric lineshapes that arise from the interacting electrons and local vibrational modes subjected to inhomogeneous broadening. In addition, the excitonic model is able to describe the expected underlying physics. However, the full spatial localisation represented by excitons might be incomplete to describe the electronic wavefunction of highly crystalline conjugated polymers such as regioregular P3HT, with possible delocalization in up to two dimensions.[21] To account for different dimensionality, the general standard critical point (SCP) lineshapes described in Chapters 4 and 5 are the natural extension. This model was shown to be superior to other analytical representations of the dielectric function of polymeric thin films. [3] It was shown that analysis of ellipsometric measurements using the SCP model gave results consistent with the anticipated physics: The electronic wavefunctions for highly crystalline films or containing chains with planar conformations displayed 1D/2D delocalization [3] in contrast to localized excitons for

amorphous polymeric films. Zhokhavets and co-workers [22] also employed a 1D density of states to describe anisotropic spin-coated thin films of poly(3-octylthiophene) (P3OT). From this model, they obtained a value of around 0.6 eV for the exciton binding energy (E_b), in fairly good agreement with E_b values obtained with other techniques. Gurau and co-workers [23] conducted a combined multi-technique study of the anisotropy of P3HT and P3OT films and used SE to correlate the spectral changes and degree of order in the films. They analyzed their data in terms of critical points using derivative spectra and tried to correlate the fine structure observed in the spectra with the local order in terms of Franck-Condon progressions. Other descriptions of the dielectric function of P3HT include explicit modelling of this fine structure by a Huang-Rhys vibronic envelope.[24] However, it has been pointed out that the Huang-Rhys description is probably too simple, not adequate to provide a satisfactory explanation of the evolution of the spectrum with local order.[23] A more complex theory has been recently developed for P3HT based on weakly coupled H-aggregates. This alternative model allows to extract relevant parameters such as an interchain bandwidth and intrachain order (conjugation length) from the polymer absorbance.[25]

As shown in Fig. 15.5 for some usual donors and acceptors, the refractive index of thin film solution processed organic semiconductor ranges between 1.7 and 2.1, while typical maximum extinction coefficients reach values about k = 1. We note that solution processed polymers may exhibit preferential molecular orientation leading to uniaxial anisotropy. The in-plane index (shown in Figure 15.5 b) is then higher than the out-of-plane (extraordinary) index.[26]

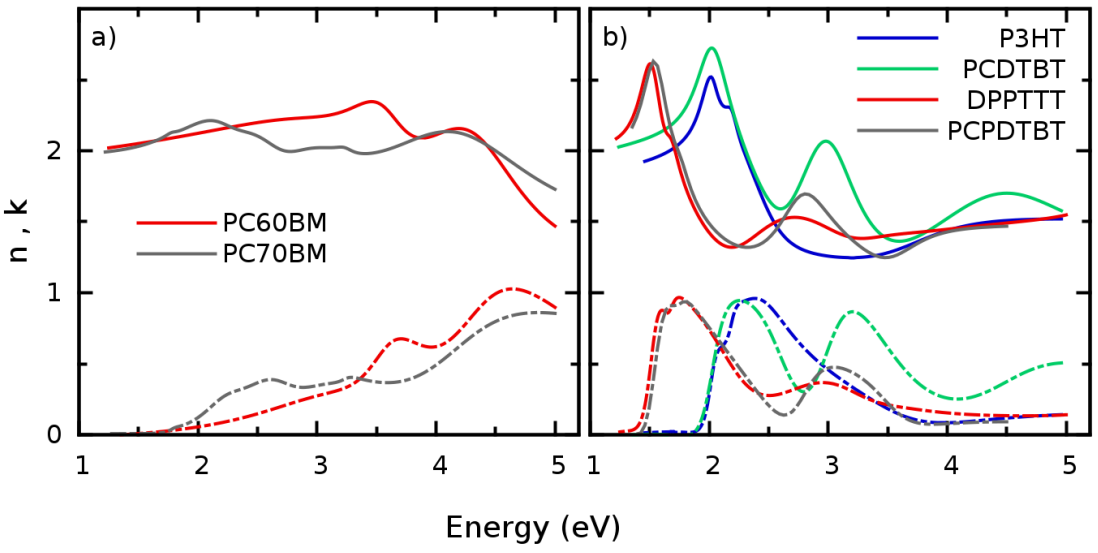

Fig. 15.5 Refractive index n and extinction coefficient k for several solution processed materials. a) acceptors b) donors.

15.3 Device Architectures

Organic photovoltaics belong to the third generation solar cell class in which a thin film of a highly absorbing direct semiconductor is sandwiched between two metals with different work functions, one of which is transparent to allow light go through. Given the aforementioned characteristics of free carrier generation in organic semiconductors, the active layer can be either a bilayer (p-n heterojunction), a bulk-heterojunction (BHJ), or a p-i-n like structure formed by embedding a mixed layer in between two layers of the pure components. These architectures are depicted in Fig. 15.6 (a), (b) and (c), respectively. While BHJs are the preferred choice for solution processed cells, active layers comprising several layers with different degrees of mixing can be obtained by thermal evaporation.

Historically, in the most conventional device architecture, often called “normal” or “standard” geometry, light reaches the active layer through the anode. In the so-called “inverted” geometry depicted in Fig. 15.6(d), light reaches the active layer through the cathode. The anode and cathode are defined by the choice of electrodes, but also, importantly, by introducing electron and hole blocking layers, respectively. The conductive polymer PEDOT:PSS is typically used as electron blocking layer which besides shifting the work function of the corresponding metal electrode, helps planarizing the surface of the contact for the correct subsequent deposition of the active layer. In the inverted structure, surfactants are used in order for the water based dispersion of PEDOT:PSS to be properly deposited on top of the typically hydrophobic active layer. Alternatively, evaporated or solution processed MoO_3 has also been used as electron blocking layer. Typical hole blocking layers include calcium, LiF, ZnO and TiOx. The latter two can be deposited using physical methods, but also from precursor solutions using wet deposition methods (from spin coating to roll-to-roll compatible slot dye coating).

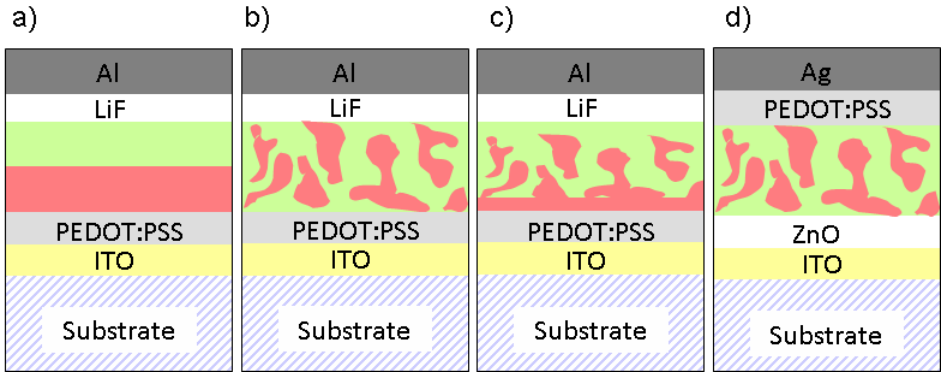

Fig. 15.6 Schematic representation of the most common device architectures. a) to c) display standard structures in which the active materials are combined in different ways, namely a) bilayer planar junction, b) bulk heterojunction, and c) combination of both as a bilayer with a wide intermixed zone. d) Inverted structure with bulk heterojunction.

In the context of device architectures, ellipsometry provides information at different levels. First, it helps to assess the structure itself, giving non-destructive estimates of thicknesses for the different layers of the stack. It also enables the monitoring of morphological aspects, such as buried interfaces, intermixing between different layers, or the appearance of phase separation between components. Finally, ellipsometry provides the required optical parameters used as input in the modeling and optimization of organic photovoltaics.

15.3.1 Vertical Structures

Within the described device architectures, vertical structure arises not only by design, as in advanced tandem organic photovoltaic cells [27] containing complex engineered multilayer stacks, but also unintentionally, in form of surface roughness, interphase boundaries and segregation within one layer, and intermixing at the interface between adjacent layers. The design of optimal devices for photovoltaic applications requires an accurate control of both the dielectric function and vertical structure because effects such as anisotropy and optical cavity interference can be dominant for light absorption in solar cells.[28,29] Rigorous modelling is crucial to improve the understanding of the internal photon conversion efficiency and allows design improvements.[30] Although some structural features like interphase mixing and segregation may be not too important to alter photonic behavior, their impact on electrical performance is significant, as they strongly affect injection and recombination properties.[31]

Evaluation of vertical structures relies on structural models built from multilayers containing effective medium approximations (EMAs) to account for the mixed layers, as described in Eq. (3.9). Typical mixed layers include surface roughness with sub-wavelength features, composed by the underlying material and void. This approximation gives good results in many situations, particularly if the rough overlayer is thinner than about 10% of the total film thickness. For thicker rough overlayers, conventional ellipsometric results may still be reliable with more complex analysis protocols and be well correlated to structural techniques. [32,33] Optical contrast is required for a successful evaluation of depth profiles by SE. For conjugated polymers, the contrast in the spectral transparency region is usually poor but the technique can take advantage of absorption contrast in films of the order of the absorption depth. Typical suitable thicknesses are in the range of 0.1 to 0.01 times the incident wavelength. In all cases, the availability of accurate reference dielectric functions eases the interpretation of the data. The study of photovoltaic devices can be simplified by examining bilayer films as model systems. Organic bilayers are often partially miscible and interlayers are generally present. Experiments that require a sharp interface can benefit from a critical validation of film structure by ellipsometry, for instance in order to determine the exciton diffusion length.[34]

Bilayers obtained by solution processing commonly have a diffuse interface because it is problematic to find orthogonal (incompatible) solvents for depositing layers sequentially. The first deposited layer may partially (or totally) dissolve when a second layer is put on top resulting in a mixed interfacial layer. Interfacial mixing can also appear to some extent for bilayers formed by thermally evaporating the top layer or after an annealing step. Ferenczi *et al.* explored interdiffusion for bilayers composed of PCBM and P3HT.[35] A solvent-free stamp transfer process was used to deposit the top PCBM layer so that the as-prepared bilayers showed sharp interfaces. Subsequent thermal annealing caused the formation of a broad mixed layer capped by a fullerene and a P3HT single component layers. The resulting triple stack showed much better performance as a photodiode than the as-prepared bilayers. Analysis of the ellipsometric data evidenced the intermixing and the obtained vertical profiles allowed to model the photodiode spectral response satisfactorily.[35]

15.3.2 Bulk Heterojunctions

The protocol to produce the technologically relevant BHJ structure, see Figs. 15.6(b) and (d), is to form a mixed layer by spin coating from a solution already containing two materials. In essence, the optical properties of the resulting blend film can be represented using an EMA such as the Bruggeman model of Eq. (3.9). In most cases, the assumptions inherent to an EMA model are justifiable. These comprise the situation that the components are well mixed (on a scale below 0.1 the wavelength) and that any additional optical excitations such as interface charge transfer have negligible spectral weight.[36] Hence, these models work well as an approximation and are very useful to deal with structural parameters. However, some basic suppositions of the EMA models might be invalid in some cases.[37,38] For instance, the mixing process may lead to domains of the pristine materials with a different microstructure than that of the single material films used to obtain reference dielectric functions. In particular, the amount of anisotropy or the extent of crystallinity have been shown to vary and are also dependent on the processing conditions. For instance, the n and k values for P3HT:PCBM blends strongly depend on annealing conditions and weight fraction, as shown in Fig. 15.7. In addition, since most organic materials are somewhat miscible,[39] for all practical purposes a ternary system is formed, made up of nearly pure domains of each material plus a fine intermixed blend of both. More refined models including those structural modifications such as effective ternary mixing [40,41] or anisotropic inclusions [42] must be used or further developed in order to find out the dielectric function of the blends from those of the constituent materials. As a matter of fact, the most accurate alternative is, probably, to consider the blend film as a different material system, comparable to an alloy system, and determine its particular dielectric function as though it was a new compound.[28,43] A helpful option for that is to build flexible material functions, like are frequently used when dealing with alloys,[38] based upon data libraries that gather diverse ways of processing reference films. In this way, satisfactory models of both the morphology and the anisotropy should be attainable and allow to deduce detailed profiles.[43] Having said

that, the heterogeneity of such films can also yield a spatial variation of the dielectric function, producing averaged results that depend to some extent on the measurement spot loci and size.

In spite of not always being the most precise description, using the dielectric function of the pristine components to model blend materials is a rather reliable procedure to investigate structural homogeneity. For example, the vertical phase separation in blends of P3HT and PCBM has been successfully evaluated using VASE [40,44,45], and the same for other photovoltaic systems such as APFO3:PCBM [38] and PCPDTBT:PC70BM.[46] For this purpose, the blend films were analyzed by decomposing the profiles in several sublayers with their corresponding dielectric functions deduced from an EMA model allowing for different compositions of the two materials. Appealingly, as-spin-coated films were seen to exhibit an intrinsic amount of vertical phase separation, and it was revealed that this segregation increased when exposing the film to temperature or solvent vapor.[44] Moreover, ellipsometry was useful to explore the dependence of the specific depth profile on a diversity of conditions related to the hydrophilicity of the substrate,[43,44] variable processing history,[44] the crystallinity of the polymer,[47] and the composition ratio of the blend,[38,45] as illustrated in Fig. 15.7. Conducting PEDOT:PSS layers with a component of un-complexed PSS were also found to exhibit vertical concentration profiles that could be characterized using ellipsometry.[48]

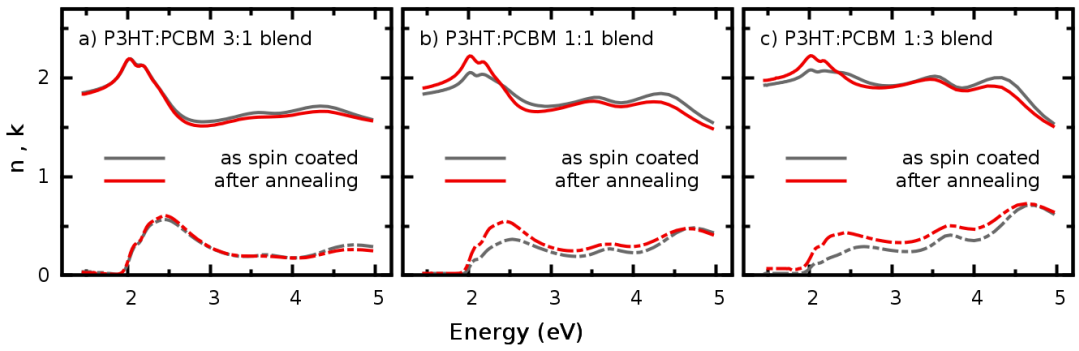

Fig. 15.7 Refractive index n and extinction coefficient k for P3HT:PCBM blends spin coated at 4000 rpm before and after 15 minutes of annealing at 140ºC. Larger changes for larger PCBM contents upon annealing are related in this case to the variation of depth profile and degree of crystallinity of the polymer.

15.3.3 Full Devices

Since ellipsometry is highly sensitive to film thickness and layer morphology, this technique is especially suited as a non invasive tool to monitor device quality. Figure 15.8 shows an example of the use of ellipsometry to assess the homogeneity of an organic photovoltaic module in inverted geometry, see Fig. 15.6 d), as it was being built. Ellipsometry was first measured at several loci over a 4 cm^2 sample after the deposition of the blocking layer (glass/ITO/ZnO), then after the deposition of the active layer

(P3HT:PCBM) and finally after the deposition of the hole conducting layer (modified PEDOT:PSS). The data clearly show that the last layer is not homogeneous and it should be reformulated to improve the wettability of PEDOT:PSS on top of the hydrophobic active layer.

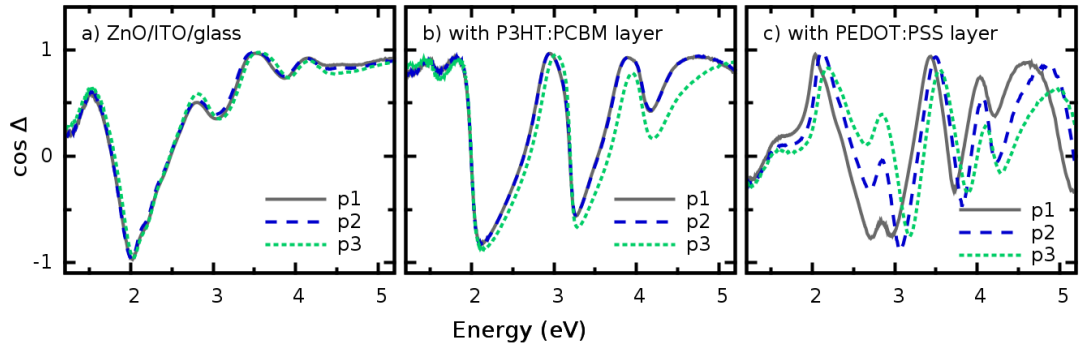

Fig. 15.8 Raw ellipsometry spectra (cos Δ) of an organic solar cell structure with inverted geometry as represented in Fig. 15.6(d). ITO was coated by sputtering and the other three layers from solution by knife coating. Measurements on three different points across the sample at various stages: a) ZnO/ITO/glass sample, b) P3HT:PCBM/ZnO/ITO/glass sample, and c) PEDOT:PSS/P3HT:PCBM/ZnO/ITO/glass sample.

A complete device often has a metallic electrode on top of the PEDOT:PSS layer deposited by thermal evaporation or screen printing. Evaluation of the full device requires, then, measuring through the glass. In this case, the available spectral range is smaller (due to the UV absorption of a ca 1mm thick glass substrate). Flexible samples are typically supported on PET substrates. These are highly anisotropic,[49] which complicates the analysis of the ellipsometric angles.

Besides quality control, ellipsometry is regularly used to obtain the input parameters that are needed in order to model and optimize the organic photovoltaic devices. Contrary to other photovoltaic technologies, charge transport in organic semiconductors is typically poor, with mobilities several orders of magnitude lower than that of amorphous silicon. This imposes a limitation with respect to how thick the active layer can be: thicker films absorb more light, but charges generated too far from the electrodes may recombine before they can be collected. The optimum film thicknesses for the multilayer stack will then be related to the absorption coefficient of the materials, electron and hole mobilities of the active layer and the degree of (unintentional) doping.[50]

In this context, ellipsometry can provide the complex refractive index for each of the relevant materials. With this input information, the electric field distribution within the active layer can be determined, and thus the profile of photogenerated excitons.[29] An electric model is then used to estimate the charge collection depending on the recombination rates and transport properties of the system. In this way, optimum film thicknesses can be determined theoretically. In most cases, the optimum thickness for the active layer corresponds to that of the first optical interference maximum for low mobility semiconductors (70nm-100nm), and to the second interference maximum for materials whose transport is better (ca 225 nm).[50-52] This type of modeling can be used to

explore also the suitability of this technology for specific applications, such as greenhouses [53] and color tunable photovoltaics for building integrated generation.[54]

15.4 Monitoring Organic Solar Cells

Ellipsometry is a non invasive and relatively fast technique (measurement time ≤1 s), and thus it is useful to monitor changes in film properties via in-situ experiments. Two main types of information can be accessed, either dynamic or thermodynamic. Examples of the former include the study of film formation from solution or the structural changes induced by post-deposition treatments. Thermodynamic aspects such as miscibility limit, phase transition temperatures or even full phase diagrams have also been investigated.

15.4.1 Monitoring Thermal Stability

In the context of bulk heterojunction solar cells, the glass transition is one of the key parameters to understand the thermal stability of the cell. If the operational temperature (up to 85ºC) is higher than the glass transition temperature, the morphology of the blend, and thus performance, will change with operation time, which is unacceptable for most applications. Providing access to the glass transition of the material in thin film form is, therefore, a very useful contribution from ellipsometry to this field. This is especially so if we consider the large number of reports that show that phase transition temperatures of geometrically confined polymers differ from the bulk values obtained by Differential Scanning Calorimetry (DSC).[55-57]

Whereas some of the studies require analysis of the full set of ellipsometric data as a function of time, it has been pointed out that for small variations in morphology or thickness (such as those typically occurring while thermally annealing), the ellipsometric angles themselves depend approximately linearly with film thickness.[4] This observation opens up the opportunity of retrieving useful pieces of information directly from the raw ellipsometry data. This includes the determination of the glass transition temperature of thin films using the kink that appears in the evolution of ψ with temperature, which reflects the different coefficients of thermal expansion before and after the glass transition.[39]

Besides the glass transition temperature, *in-situ* ellipsometry can be employed to characterize thoroughly the phase evolution in quasi-isothermal experiments, including the determination of crystallization and liquid crystalline temperatures. Some examples in the literature include PFO,[55] F8BT,[55] P3HT,[58] APFO3,[56] APFO9,[56] pBTTT,[59] and PCDTBT.[60] The full phase diagram for photovoltaic blends consisting of the low band gap polymer APFO3 and fullerene (PCBM) were deduced using ellipsometry in combination with polarized microscopy.[39] For this, the temperature dependence of the ellipsometric angles was recorded for several polymer: fullerene compositions. The phase diagram was then constructed and revealed a eutectic behavior

including a lyotropic phase. This study provided information on the miscibility limit of both compounds, and demonstrated that the miscibility limit depends on the molecular weight of the polymer. The authors correlated the high glass transition temperatures with the high thermal stability of the corresponding devices and also the miscibility limit with the recombination probability for the blends.

15.4.2 Monitoring Morphology Evolution

As it has been mentioned throughout this chapter, the way in which donor and acceptor molecules pack in the solid state to form the blend film is a critical aspect for the operation of organic photovoltaics. The two materials should form a finely interpenetrated network to allow charge generation and extraction. Optimum domain sizes are around 10-20 nm, furthermore, the domain purity is crucial to avoid charge recombination leading to performance loss. Being so critical, a myriad of methods to control the film morphology have emerged. These include control of the drying kinetics during solution deposition via solvent mixtures, use of solvent saturated atmospheres, varying stage or solution temperature, or the use of additives. Alternatively, the structure of some blend films can be modified after deposition using treatments such as thermal or vapor annealing.

The time scales of deposition and post deposition treatments are very different, being a few seconds for the former, and several minutes for the later. In both cases, in-situ ellipsometry can offer insights into morphology evolution, as exemplified in Fig. 15.9. This is because the optical features associated to isolated molecules, molecular aggregates and crystalline domains are all different.

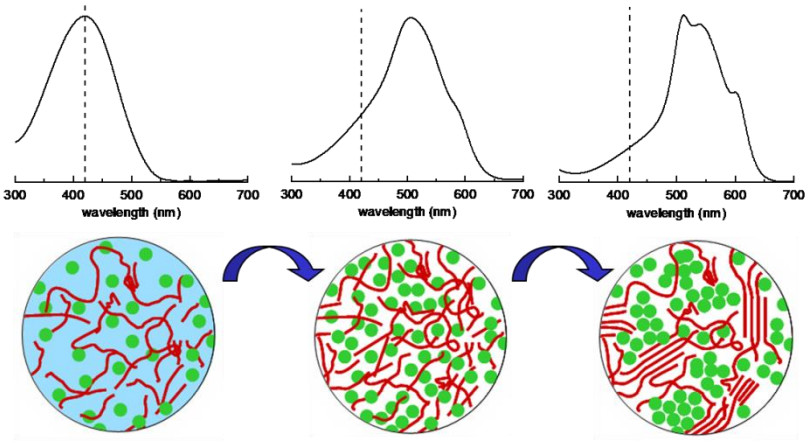

Fig. 15.9 Schematic representation of the evolution of a polymer-fullerene blend upon thermal annealing. The spectra illustrate qualitative changes in extinction coefficient curves that may help to monitor morphology changes in real time.

For the workhorse bulk heterojunction material system P3HT:PCBM, ellipsometric studies have been carried out by exposing the films to saturated atmosphere of solvent vapor.[44] The ellipsometric data exhibited variations due to changes in oscillator

strength and density, which were used to deduce the onset of polymer crystallization. Subsequent lateral and vertical diffusion of fullerene molecules [44,45,61] yielded finally a blend structure offering superior solar cell performance. Similarly, Wang *et al.*[62] have ellipsometrically monitored the evolution of these blends upon thermal annealing. Three distinct regimes were identified. First, the solvent trapped within the film evaporated, followed by the polymer crystallization and finally, the phase separation of the two components.

The bilayer geometry constitutes a useful system to study microstructure evolution. In this case, two layers of the pure constituents are deposited sequentially, typically first the polymer and then the fullerene from an orthogonal solvent or thermally evaporated on top of the polymer film. This system is valuable because the starting point is very well defined (pure vertical domains of each component) and then upon application of an external stimulus, such as temperature, the morphology evolves. The kinetics of molecular diffusion, as well as the miscibility limit have been studied by measuring ellipsometry on bilayers.[35,63] In a study comprising two polymers and four different fullerenes, ellipsometry enabled to understand how mixing only occurred above the glass transition of the polymer, and was consistent with swelling of the polymer by the fullerene.[63] For absorbing materials, the limitation here is that films ought to be thin enough to enable optical access to the bottom layer. The use of ellipsometry to investigate polymer film swelling by penetrants has been recently reviewed by Ogieglo and colleagues.[64]

The characterization of thin film changes during fast deposition processes is yet more challenging due to the very wide timescales (from milliseconds to minutes) and the fast changing film properties, starting from the few microns thick wet film down to the 100 nm thick dried film. Other deposition methods have also been explored, such as dip coating [65] (see Fig. 15.10) and knife coating [66,67]. It is worth noting that high speed photometry was also used to monitor the spin-coating process of non-conjugated polymer blends.[68] Polarized photometry has also allowed to monitor the layer-by-layer growth of small molecule films.[69]

The drying kinetics of a knife-coated P3HT:PCBM film was explored by combining in-situ ellipsometry and X-ray measurements.[66] This encouraging report revealed different steps in film formation. In the wet film, the polymer chains start to crystallize by way of heterogeneous nucleation when the concentration of polymer surpasses 50%. Due to the remaining solvent, a self-annealing step takes place. This evolution is monitored by following the ellipsometrically deduced film thickness and extinction coefficients. As a first approximation, the changes in thickness and refractive index during annealing or in the last stages of film formation can be rationalized in terms of variations in film density (ρ) and polarizability (μ).[61,65,70] For a given system with an accessible transparent spectral window, the variation in refractive index far from the absorption edge can be approximated as:

$$\frac{n_t^2 - 1}{n_0^2 - 1} \cong \frac{\mu_t \rho_t}{\mu_0 \rho_0} \qquad (15.1)$$

Equation (15.1) has been used to correlate the values of density and polarizability with the length of the polymer side chains in different films,[71] and to compare the values before and after thermal annealing [44,71] as well as during deposition.[65] For the case of post-deposition treatments, the film mass at two given times has to be conserved, and then the previous equation can be rewritten as:

$$\frac{n_t^2 - 1}{n_{t=0}^2 - 1} \cdot \frac{d_t}{d_{t=0}} \cong \frac{\mu_t}{\mu_{t=0}} \qquad (15.2)$$

By analyzing the time dependent ellipsometry data, the refractive index and thickness can be found independently. Then, this relationship allows to estimate the polarizability variations occurring during a post deposition treatment and correlate them to the morphology of the film. These variations may be originated, for instance, by the evolution of the average degree of molecular orientation upon annealing.[65]

Clearly, the development of in-situ ellipsometry for the characterization of organic solar cells films during deposition or annealing is at an early stage, so far. The very reassuring already reported results, however, encourage further investigations to cast light into such topics as the effect of additives, molecular weight, or crystallization tendency.

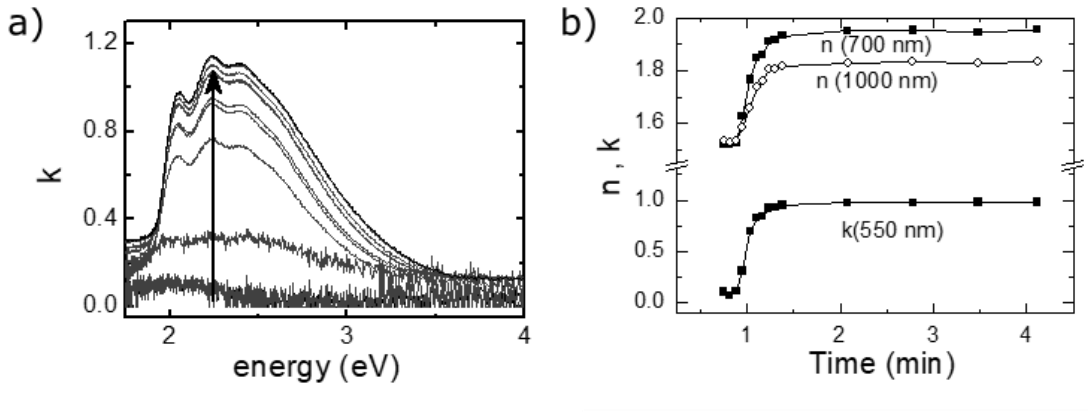

Fig. 15.10 Dependence of the optical constants of a P3HT film upon drying. a) Spectral changes of the extinction coefficient. The arrow marks the wavelength of maximum absorption, 550nm. b) Time evolution of *n* and *k* at selected wavelengths.

15.4.3 Monitoring Fabrication

Besides the great sensitivity to small thickness and/or dielectric function changes, the new generation of commercially available ellipsometers equipped with CCD detection are also very fast, with acquisition times around 50 ms. In-situ characterization of layers and stacks *in-line* during roll-to-roll processing has, therefore, become a reality.

Indeed, two groups have already built stand alone in-line ellipsometers into lab scale roll-to-roll systems devoted to the fabrication of organic photovoltaics.[1,2] The advancements introduced by one such system have been protected via patent filing.[72] Very fast data acquisition, processing and analysis are key features of these pieces of equipment. In order to have access to the full width of the rolling web, the optics of the ellipsometer are scanned (translated) perpendicularly to the roll to roll moving direction. Alternatively, an expanded beam geometry coupled to a 2D detector with no moving parts has also been proposed for in-line quality monitoring during roll-to-roll manufacturing.[73]

15.4.4 Monitoring Degradation

Stability is one of the key challenges to overcome before organic photovoltaics can reach the market. Besides the aforementioned thermal stability, photodegradation and chemical stability need to be addressed. Interestingly, most common degradation pathways affecting the active layer in OPVs, such as chain scission or shortening, conjugation breaking via defects, etc, result in a reduction of conjugation length, yielding blue shifted absorption and loss in vibronic sideband spectral resolution. The absorption spectrum, therefore, reflects the degree of degradation of a given material. Note, cautiously, that the electronic processes are affected by degradation much more strongly via trap formation, in such a way that an absorption loss of less than 3% might be associated to the same degree of degradation than a solar cell efficiency loss of 80%.

In a pioneering work on photooxidation of polythiophenes from 1994, Arwin and Jansson proposed the ex-situ ellipsometric determination of the absorption coefficient as an easy magnitude measurement to detect degradation.[20] They observed how photodegradation resulted in a loss of oscillator strength, and a broadening of absorption. Similar studies have been conducted on other polymers, such as MHPPV [74] and small molecules, such as Alq3.[75] The structural stability of polymer/fullerene blends has also been assessed via ellipsometry.[76] These authors find that the vertical composition profile evolves over time, with fullerene molecules accumulating at the surface. This has a clear effect on the corresponding solar cells as a fullerene rich interface can act as an electron conducting layer.

There is plenty of room for further studies of the stability in this type of systems. In particular, in-situ real time investigation of the degradation of photovoltaic systems under controlled oxygen, humidity and temperature conditions might prove very useful. In the case of lead halide perovskite based hybrid photovoltaics, ellipsometry has been used in-situ while exposing the material to water vapor [77] revealing a reversible hydration process. Similar studies applied to organic photovoltaics will help to increase our understanding of the degradation pathways and how to cut them short.

15.5 Hybrid Approaches

For the sake of completeness, we mention briefly the use of ellipsometry for characterization of hybrid active layers in solar cells. Current organic-inorganic mixed approaches evolved from the concept of dye-sensitized solar cells. These electrochemical or Grätzel cells are composed by a mesoporous titania matrix with a thin layer of dye attached to the surface and embedded in an electrolyte solution. The thickness and porosity of the mesoporous TiO_2 have a relevant effect on the cell performance and can be characterized by ellipsometry.[78] Evolution of this concept to solid state brings hybrid approaches closer to the concept of bulk heterojunctions, like that represented in Fig. 15.1(c) where a hole-transporting polymer (frequently spiro-MeOTAD) replaces the electrolyte. In other studies, infiltration of a donor polymer to replace both the dye and the electrolyte has been considered, where the inorganic semiconductor TiO_2 acts as the acceptor. These vertically mixed heterojunctions are efficiently characterized by SE [78] also in this case. Another widely used acceptor is ZnO. Optical properties of blends between ZnO and several polymers such as P3HT have been investigated by SE and have been successfully correlated to the color of full devices.[79] Effective medium approximations have been applied to study structural aspects in polymer-quantum dot blend films [80] which are also used in hybrid solar cell concepts. Last but not least, lead halide perovskite-based solar cells evolved from the same hybrid concept. Chapter 16 is devoted to this hybrid kind of solar cells due to the current enormous interest and intense activity in this field of research.

15.6 Summary

In this chapter we have reviewed a representative selection of significant examples regarding the use of spectroscopic ellipsometry for the characterization of organic semiconductors applied to solar cells. Throughout the chapter, we have detailed the particularities of organic semiconductors that ultimately define the device architectures and indicated which aspects can be characterized by ellipsometry both regarding material preparation and device structure. First, we have described the ellipsometric characterization of single-phase materials that form the active layers of OPVs including single crystals and films of small molecules and polymers. We have further outlined the use of ellipsometry for the characterization of device-quality layers such as films with vertical structure, either a single blend layer or sequentially deposited layers. Also, we have pointed out the real time *in situ* application of ellipsometry to monitor film deposition processes and post-deposition treatments. Finally, we have commented on characterization aspects of organic-inorganic hybrid solar cell materials. In all cases, an accurate knowledge of the dielectric functions of the materials, enabled by the use of ellipsometry, is essential to understand and model the optoelectronic properties of photovoltaic devices. Moreover, advanced ellipsometry can provide fundamental information about the structural configuration of the thin films, along with the phase

separation of components, the quality of interfaces, and characteristics of molecular kinetics for the fabrication processes.

Acknowledgments

The authors thank Ms. Andrea Pitillas help in the preparation of devices studied in Fig. 15.8 and the Spanish Ministry of Economy and Competitiveness for funding through grants MAT2012-37776, MAT2015-70850-P, and the "Severo Ochoa" Programme for Centres of Excellence in R&D (SEV-2015-0496).

References

1. M. V. Madsen, K. O. Sylvester-Hvid, B. Dastmalchi, K. Hingerl, K. Norrman, T. Tromholt, M. Manceau, D. Angmo, and F. C. Krebs, *J. Phys.Chem. C* **115**, 10817 (2011)

2. S. Logothetidis, D. Georgiou, A. Laskarakis, C. Koidis, and N. Kalfagiannis, *Sol. Ener. Mater. Sol. Cells* **112**, 144 (2013)

3. M. Campoy-Quiles, J. Nelson, D. D. C. Bradley, and P. G. Etchegoin, *Phys. Rev. B* **76**, 235206 (2007)

4. M. Campoy-Quiles, M. I. Alonso, D. D. C. Bradley, and L. J. Richter, *Adv. Funct. Mater.* **24**, 2116 (2014)

5. S. Tavazzi, L. Raimondo, L. Silvestri, P. Spearman, A. Camposeo, M. Polo, and D. Pisignano, *J. Chem. Phys.* **128**, 154709 (2008)

6. D. Faltermeier, B. Gompf, M. Dressel, A. K. Tripathi, and J. Pflaum, *Phys. Rev. B* **74**, 125416 (2006)

7. P. Milani, M. Manfredini, G. Guizzetti, F. Marabelli, and M. Patrini, *Solid State Commun.* **90**, 639 (1994)

8. M.I. Alonso and M. Garriga, *Thin Solid Films* **455-456**, 124 (2004)

9. O. Arteaga, M. Garriga, and M. I. Alonso, unpublished (2017)

10. L. Gisslén and R. Scholz, *Phys. Rev. B* **80**, 115309 (2009)

11. M. I. Alonso, M. Garriga, J.O. Ossó, F. Schreiber, and R. Scholz, *Thin Solid Films* **571, Part 3**, 420 (2014)

12. C. Schünemann, D. Wynands, L. Wilde, M. P. Hein, S. Pfützner, C. Elschner, K.-J. Eichhorn, K. Leo, and M. Riede, *Phys. Rev. B* **85**, 245314 (2012)

13. U. Heinemeyer, A. Hinderhofer, M. I. Alonso, J. O. Ossó, M. Garriga, M. Kytka, A. Gerlach, and F. Schreiber, *Phys. Status Solidi A* **205**, 927 (2008)

14. C. Schünemann, D. Wynands, K.-J. Eichhorn, M. Stamm, K. Leo, and M. Riede, *J. Phys.Chem. C* **117**, 11600 (2013)

15. G. Chen, D. Yokoyama, H. Sasabe, Z. Hong, Y. Yang, and J. Kido, *Appl. Phys. Lett.* **101**, 083904 (2012)

16. L.-Y. Lin, Y.-H. Chen, Z.-Y. Huang, H.-W. Lin, S.-H. Chou, F. Lin, C.-W. Chen, Y.-H. Liu, and K.-T. Wong, *J. Am. Chem. Soc.* **133**, 15822 (2011)

17. M. I. Alonso, M. Garriga, J. O. Ossó, F. Schreiber, E. Barrena, and H. Dosch, *J. Chem. Phys.* **119**, 6335 (2003)

18. H. Gommans, T. Aernouts, B. Verreet, P. Heremans, A. Medina, C. G. Claessens, and T. Torres, *Adv. Funct. Mater.* **19**, 3435 (2009)

19. F. C. Spano and C. Silva, *Annu. Rev. Phys. Chem.* **65**, 477 (2014)

20. H. Arwin and R. Jansson, *Electrochim. Acta* **39**, 211 (1994)

21. R. Osterbacka, C. P. An, X. M. Jiang, and Z. V. Vardeny, *Science* **287**, 839 (2000)

22. U. Zhokhavets, R. Goldhahn, G. Gobsch, and W. Schliefke, *Synth. Met.* **138**, 491 (2003)

23. M. C. Gurau, D. M. Delongchamp, B. M. Vogel, E. K. Lin, D. A. Fischer, S. Sambasivan, and L. J. Richter, *Langmuir* **23**, 834 (2007)

24. A. J. Morfa, T. M. Barnes, A. J. Ferguson, D. H. Levi, G. Rumbles, K. L. Rowlen, and J. van de Lagemaat, *J. Pol. Sci. B: Pol. Phys.* **49**, 186 (2011)

25. J. Clark, J.-F. Chang, F. C. Spano, R. H. Friend, and C. Silva, *Appl. Phys. Lett.* **94**, 163306 (2009)

26. M. Campoy-Quiles, P. G. Etchegoin, and D. D. C. Bradley, *Phys. Rev. B* **72**, 045209 (2005)

27. T. Ameri, G. Dennler, C. Lungenschmied, and C. J. Brabec, *Energy & Environmental Science* **2**, 347 (2009)

28. N. K. Persson, H. Arwin, and O. Inganäs, *J. Appl. Phys.* **97**, 034503 (2005)

29. L. A. A. Pettersson, L. S. Roman, and O. Inganäs, *J. Appl. Phys.* **86**, 487 (1999)

30. G. F. Burkhard, E. T. Hoke, S. R. Scully, and M. D. McGehee, *Nano Lett.* **9**, 4037 (2009)

31. L.-M. Chen, Z. Hong, G. Li, and Y. Yang, *Adv. Mater.* **21**, 1434 (2009)

32. M. Akagawa and H. Fujiwara, *J. Appl. Phys.* **110**, 073518 (2011)

33. D. Lehmann, F. Seidel, and D. R. T. Zahn, *Springerplus* **3**, 82 (2014)

34. J. D. A. Lin, O. V. Mikhnenko, J. Chen, Z. Masri, A. Ruseckas, A. Mikhailovsky, R. P. Raab, J. Liu, P. W. M. Blom, M. A. Loi, C. J. Garcia-Cervera, I. D. W. Samuel, and T.-Q. Nguyen, *Mater. Horiz.* **1**, 280 (2014)

35. T. A. M. Ferenczi, J. Nelson, C. Belton, A. M. Ballantyne, M. Campoy-Quiles, F. M. Braun, and D. D. C. Bradley, *J. Phys. Condens. Matter* **20**, 475203 (2008)

36. K. Vandewal, K. Tvingstedt, A. Gadisa, O. Ingänas, and J. V. Manca, *Nat. Mater.* **8**, 904 (2009)

37. U. Zhokhavets, R. Goldhahn, G. Gobsch, M. Al-Ibrahim, H. K. Roth, S. Sensfuss, E. Klemm, and D. A. M. Egbe, *Thin Solid Films* **444**, 215 (2003)

38. M. Campoy-Quiles, C. Müller, M. Garriga, E. Wang, O. Inganäs, and M. I. Alonso, *Thin Solid Films* **571, Part 3**, 371 (2014)

39. C. Müller, J. Bergqvist, K. Vandewal, K. Tvingstedt, A. S. Anselmo, R. Magnusson, M. I. Alonso, E. Moons, H. Arwin, M. Campoy-Quiles, and O. Inganäs, *J. Mater. Chem.* **21**, 10676 (2011)

40. I. Burgues-Ceballos, M. Campoy-Quiles, L. Francesch, and P. D. Lacharmoise, *J. Pol. Sci. B: Pol. Phys.* **50**, 1245 (2012)

41. S. Engmann, V. Turkovic, P. Denner, H. Hoppe, and G. Gobsch, *J. Pol. Sci. B: Pol. Phys.* **50**, 1363 (2012)

42. S. Engmann, V. Turkovic, G. Gobsch, and H. Hoppe, *Adv. Ener. Mater.* **1**, 684 (2011)

43. D. S. Germack, C. K. Chan, R. J. Kline, D. A. Fischer, D. J. Gundlach, M. F. Toney, L. J. Richter, and D. M. DeLongchamp, *Macromolecules* **43**, 3828 (2010)

44. M. Campoy-Quiles, T. Ferenczi, T. Agostinelli, P. G. Etchegoin, Y. Kim, T. D. Anthopoulos, P. N. Stavrinou, D. D. C. Bradley, and J. Nelson, *Nat. Mater.* **7**, 158 (2008)

45. T. Agostinelli, S. Lilliu, J. G. Labram, M. Campoy-Quiles, M. Hampton, E. Pires, J. Rawle, O. Bikondoa, D. D. C. Bradley, T. D. Anthopoulos, J. Nelson, and J. E. Macdonald, *Adv. Funct. Mater.* **21**, 1701 (2011)

46. A. Guerrero, B. Doerling, T. Ripolles-Sanchis, M. Aghamohammadi, E. Barrena, M. Campoy-Quiles, and G. Garcia-Belmonte, *ACS Nano* **7**, 4637 (2013)

47. M. Campoy-Quiles, V. Randon, M. Mróz, M. Jarzaguet, M. Garriga, and J. Cabanillas-González, *Organic Photonics and Photovoltaics* **1**, 11 (2013)

48. T. Ino, T. Hayashi, T. Fukuda, K. Ueno, and H. Shirai, *Phys. Status Solidi C* **8**, 3025 (2011)

49. S. Logothetidis, "Polymeric substrates and encapsulation for flexible electronics: Bonding structure, surface modification and functional nanolayer growth," *Rev. Adv. Mater. Sci.* **10**, 387 (2005)

50. F. Deledalle, T. Kirchartz, M. S. Vezie, M. Campoy-Quiles, P. Shakya Tuladhar, J. Nelson, and J. R. Durrant, *Phys. Rev. X* **5**, 011032 (2015)

51. D. W. Sievers, V. Shrotriya, and Y. Yang, *J. Appl. Phys.* **100**, 114509 (2006)

52. A. J. Moulé, J. B. Bonekamp, and K. Meerholz, *J. Appl. Phys.* **100**, 094503 (2006)

53. C. J. M. Emmott, J. A. Rohr, M. Campoy-Quiles, T. Kirchartz, A. Urbina, N. J. Ekins-Daukes, and J. Nelson, *Energy Environ. Sci.* **8**, 1317 (2015)

54. R. Betancur, P. Romero-Gomez, A. Martinez-Otero, X. Elias, M. Maymó, and J. Martorell, *Nature Photon.* **7**, 995 (2013)

55. M. Campoy-Quiles, M. Sims, P. G. Etchegoin, and D. D. C. Bradley, *Macromolecules* **39**, 7673 (2006)

56. C. Müller, L. M. Andersson, O. Peña-Rodriguez, M. Garriga, O. Inganäs, and M. Campoy-Quiles, *Macromolecules* **46**, 7325 (2013)

57. A. Roigé, M. Campoy-Quiles, J. O. Ossó, M. I. Alonso, L. F. Vega, and M. Garriga, *Synth. Met.* **161**, 2570 (2012)

58. D. Cheyns, K. Vasseur, C. Rolin, J. Genoe, J. Poortmans, and P. Heremans, *Nanotechnology* **19**, 424016 (2008)

59. D. M. DeLongchamp, R. J. Kline, Y. Jung, E. K. Lin, D. A. Fischer, D. J. Gundlach, S. K. Cotts, A. J. Moad, L. J. Richter, M. F. Toney, M. Heeney, and I. McCulloch, *Macromolecules* **41**, 5709 (2008)

60. T. Wang, A. Pearson, A. D. F. Dunbar, P. A. Staniec, D. C. Watters, D. Coles, H. Yi, A. Iraqi, D. G. Lidzey, and R. A. L. Jones, *Eur. Phys. J. E* **35**, 129 (2012)

61. D. Nassyrov, C. Mueller, A. Roigé, I. Burgues-Ceballos, J. O. Ossó, D. B. Amabilino, M. Garriga, M. I. Alonso, A. R. Goñi, and M. Campoy-Quiles, *J. Mater. Chem.* **22**, 4519 (2012)

62. T. Wang, A. J. Pearson, D. G. Lidzey, and R. A. L. Jones, *Adv. Funct. Mater.* **21**, 1383 (2011)

63. D. Leman, M. A. Kelly, S. Ness, S. Engmann, A. Herzing, C. Snyder, H. W. Ro, R. J. Kline, D. M. DeLongchamp, and L. J. Richter, *Macromolecules* **48**, 383 (2015)

64. W. Ogieglo, H. Wormeester, K.-J. Eichhorn, M. Wessling, and N. E. Benes, *Progress in Polymer Science* **42**, 42 (2015)

65. M. Campoy-Quiles, M. Schmidt, D. Nassyrov, O. Peña, A. R. Goñi, M. I. Alonso, and M. Garriga, *Thin Solid Films* **519**, 2678 (2011)

66. T. Wang, A. D. F. Dunbar, P. A. Staniec, A. J. Pearson, P. E. Hopkinson, J. E. MacDonald, S. Lilliu, C. Pizzey, N. J. Terrill, A. M. Donald, A. J. Ryan, R. A. L. Jones, and D. G. Lidzey, *Soft Matter* **6**, 4128 (2010)

67. B. Schmidt-Hansberg, M. F. G. Klein, K. Peters, F. Buss, J. Pfeifer, S. Walheim, A. Colsmann, U. Lemmer, P. Scharfer, and W. Schabel, *J. Appl. Phys.* **106**, 124501 (2009)

68. S. Y. Heriot and R. A. L. Jones, *Nat. Mater.* **4**, 782 (2005)

69. U. Heinemeyer, K. Broch, A. Hinderhofer, M. Kytka, R. Scholz, A. Gerlach, and F. Schreiber, *Phys. Rev. Lett.* **104**, 257401 (2010)

70. S. Heun, R. F. Mahrt, A. Greiner, U. Lemmer, H. Bassler, D. A. Halliday, D. D. C. Bradley, P. L. Burn, and A. B. Holmes, *J. Phys. Condens. Matter* **5**, 247 (1993)

71. T. Kreouzis, D. Poplavskyy, S. M. Tuladhar, M. Campoy-Quiles, J. Nelson, A. J. Campbell, and D. D. C. Bradley, *Phys. Rev. B* **73**, 235201 (2006)

72. S. Logothetidis, Method for in-line determination of film thickness and quality during printing processes for the production of organic electronics, 2014, US Patent App. 14/113,125.

73. A. Shan, M. Fried, G. Juhasz, C. Major, O. Polgar, A. Nemeth, P. Petrik, L.R. Dahal, Jie Chen, Zhiquan Huang, N.J. Podraza, and R.W. Collins, *IEEE J. Photovolt.* **4**, 355 (2014)

74. R. F. Bianchi, D. T. Balogh, M. Tinani, R. M. Faria, and E. A. Irene, *J. Pol. Sci. B: Pol. Phys.* **42**, 1033 (2004)

75. S. Kumar, V. K. Shukla, and A. Tripathi, *Thin Solid Films* **477**, 240 (2005)

76. S. Engmann, V. Turkovic, H. Hoppe, and G.Gobsch, *Synth. Met.* **161**, 2540 (2012)

77. A. M. A. Leguy, Y. Hu, M. Campoy-Quiles, M. I. Alonso, O. J. Weber, P. Azarhoosh, M. van Schilfgaarde, M. T. Weller, T. Bein, J. Nelson, P. Docampo, and P. R. F. Barnes, *Chem. Mater.* **27**, 3397 (2015)

78. A. J. Moulé, H. J. Snaith, M. Kaiser, H. Klesper, D. M. Huang, M. Grätzel, and K. Meerholz, *J. Appl. Phys.* **106**, 073111 (2009)

79. D. Duché, F. Bencheikh, S. Ben Dkhil, M. Gaceur, N. Berton, O. Margeat, J. Ackermann, J.J. Simon, and L. Escoubas, *Sol. Ener. Mater. Sol. Cells* **126**, 197 (2014)

80. M. Schädel, K. F. Jeltsch, P. Niyamakom, F. Rauscher, Y. Zhou, M. Krüger, and K. Meerholz, *J. Pol. Sci. B: Pol. Phys.* **50**, 75 (2012)